

The potential of SiO₂:Al³⁺,Eu²⁺ blue phosphor coatings in greenhouse application

Cho, Chun-Ting; Bosco, Giacomo; van der Kolk, Erik

DOI

[10.1016/j.optmat.2024.116047](https://doi.org/10.1016/j.optmat.2024.116047)

Publication date

2024

Document Version

Final published version

Published in

Optical Materials

Citation (APA)

Cho, C.-T., Bosco, G., & van der Kolk, E. (2024). The potential of SiO₂:Al³⁺,Eu²⁺ blue phosphor coatings in greenhouse application. *Optical Materials*, 157, Article 116047. <https://doi.org/10.1016/j.optmat.2024.116047>

Important note

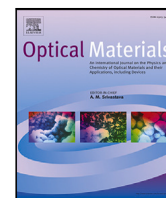
To cite this publication, please use the final published version (if applicable). Please check the document version above.

Copyright

Other than for strictly personal use, it is not permitted to download, forward or distribute the text or part of it, without the consent of the author(s) and/or copyright holder(s), unless the work is under an open content license such as Creative Commons.

Takedown policy

Please contact us and provide details if you believe this document breaches copyrights. We will remove access to the work immediately and investigate your claim.



Research article

The potential of $\text{SiO}_2:\text{Al}^{3+}, \text{Eu}^{2+}$ blue phosphor coatings in greenhouse application

Chun-Ting Cho ^{a,*}, Giacomo Bosco ^b, Erik van der Kolk ^a

^a *Luminescence Materials, Delft University of Technology, Mekelweg 15, Delft, The Netherlands*

^b *FOTONIQ, Ampèreweg 16, Delft, The Netherlands*

ARTICLE INFO

Keywords:

Europium
Aluminum
Silicon
Luminescence
Energy transfer
Greenhouse

ABSTRACT

Solar spectral conversion by a low-cost luminescent coating for greenhouse applications increases crop yield and can contribute to addressing the food crisis. A luminescent coating based on cheap SiO_2 particles doped with Eu^{2+} and Al^{3+} demonstrated extra photosynthetic active radiation (PAR) in this work. To optimize the efficiency of this phosphor for greenhouse applications, three phosphor series with varying Al/Eu content in SiO_2 were synthesized via a sol-gel approach and characterized by luminescence decay time, absorption, luminescent excitation, emission, and quantum yield measurements. With increasing the Eu%, at a fixed Al%, the decay time and quantum yield decreased while the emission shifted to the red. The effect can be explained by a more and more efficient resonance energy transfer to lower energy Eu^{2+} ions and quenching sites. While increasing the Al% at a fixed Eu%, the decay time and quantum yield increased, and the red-shift was reduced. Both effects can be explained by an enhanced Eu^{2+} solubility (reduced Eu clustering) through the Al^{3+} co-doping, causing the average Eu^{2+} - Eu^{2+} distance to be longer and the onset of concentration quenching to shift to a higher Eu%. Specifically, we found that for 1 mol% Eu^{2+} , a minimum of 4 mol% Al^{3+} was required to avoid concentration quenching. Two indicators were developed to quantify the UV to PAR converting efficiency and to quantify the PAR transmission enhancement. Both indicators were determined in a real coating sample based on the optimized phosphor. The result showed an additional PAR was provided by our luminescent coating. A general discussion about all factors that can bring the conversion efficiency of a phosphor coating closer to the theoretical maximum will be presented.

1. Introduction

According to the 2023 report from the Global Network Against Food Crises, food insecurity is threatening more than 238 million people all over the world [1]. This crisis will become severe due to climate change causing extreme weather and, in the longer run, rising sea levels [2]. How to produce more food in less area is turning into a global economic issue. Greenhouses can provide a solution as they have a much higher production yield per surface area compared to open land growth and provide independence to weather conditions.

The amount of light (flux) projected on plants has a large impact on the yield. The concept of “1% extra light leads to 1% extra crop yield” is widely accepted in the horticulture field [3]. Greenhouse owners, therefore, often utilize artificial lighting, such as high-pressure sodium lamps and LEDs, not only to increase photon flux but also to adjust the light spectrum for specific growing stages [3–7]. As these techniques consume energy, it is worthwhile to consider a photoluminescent material that converts ultraviolet (UV) solar radiation to photosynthetic

active radiation (PAR) as an alternative solution for spectral conversion or extra light since UV is unused in photosynthesis [8–10].

An economically viable spectral conversion coating must be based on a cheap phosphor. Silicon dioxide (SiO_2) is a popular host matrix in the industry due to its excellent chemical stability and low production cost. Doping with Eu^{2+} turns SiO_2 into a blue emitting phosphor that absorbs UV light but no PAR, seemingly ideal for UV to PAR conversion and a subsequent enhanced PAR transmission [11–13]. Unfortunately, a significant limitation observed in this material is that Eu^{2+} is limited to low doping concentration when incorporated into the SiO_2 host because lanthanide ions can only create their own crystallographic interstitial sites due to the size and charge mismatch. The resulting low solubility limit leads to a lower luminescent intensity due to concentration quenching, even more so due to clustering of lanthanide (Ln) ions [14–16]. For example, research from Lochhead et al. has shown that clustering of Eu^{3+} in SiO_2 already happens at 0.3 mol% [17]. Co-doping SiO_2 with ions like Al, P, Ba, or Mg has

* Corresponding author.

E-mail address: c.cho@tudelft.nl (C.T. Cho).

<https://doi.org/10.1016/j.optmat.2024.116047>

Received 20 June 2024; Received in revised form 13 August 2024; Accepted 1 September 2024

Available online 5 September 2024

0925-3467/© 2024 The Author(s). Published by Elsevier B.V. This is an open access article under the CC BY license (<http://creativecommons.org/licenses/by/4.0/>).

successfully been used to increase the solubility of Ln ions [18–21]. Co-doping with Al has appeared especially beneficial for increasing Eu²⁺ luminescent intensity [22–24].

The mechanism of how co-doping with Al³⁺ helps increase the solubility limit of trivalent lanthanides in the SiO₂ host was described by Lægsgaard using density function theory (DFT) to predict the local structure around Er³⁺ ions in silica-alumina oxide [25]. On the other hand, Funabiki et al. explained the co-doping theory from a thermodynamic point of view by the formation of a solvation shell [26]. The formation of the Al-Ln complex increases system entropy and suppresses Ln clustering. Nogami et al. proved that co-doping Al³⁺ in SiO₂ enhances the luminescent intensity of Eu²⁺ by 250-fold [23]. Kishimoto et al. studied the Eu²⁺ quantum efficiency while tuning the Al and Eu content between 0%–10% and 0%–5%, respectively. They concluded that 1 wt% Eu₂O₃ in 1Al₂O₃-99SiO₂ glass gave the highest quantum efficiency of 48% [24].

Because a greenhouse coating requires the highest possible UV absorption in a coating of limited practical thickness, we report in this work a synthesis that increases absorption by raising Eu²⁺ doping content without lowering the quantum efficiency and subsequently applying the best phosphor particles in a real greenhouse coating. To achieve this, three sample series with a varying Eu%, a varying Al%, and a fixed Al/Eu ratio were synthesized via a base-catalyzed sol-gel method [27,28]. Due to the lack of published work quantifying the efficiency of a greenhouse coating, two efficiency indicators are presented [29,30]. The first is to quantify the UV to PAR conversion efficiency, and the second is the PAR transmission enhancement. The results allowed us to discuss relevant processes that determine the success of a spectral-converting greenhouse coating.

2. Experiments

2.1. Phosphor preparation

All samples were synthesized via the sonochemical sol-gel method. A stoichiometric amount of aluminum isopropoxide Al(O-i-Pr)₃ (Sigma-aldrich, ≥ 98%) was added into pure ethanol, and europium nitrate Eu(NO₃)₃ (ABCR, 99.9%) was added into deionized (DI) water respectively according to the molar ratio of the sample composition. After the precursors were completely dissolved, the two solutions were added into tetraethyl orthosilicate TEOS (ABCR, 99%) solution, the source of Si, with pure ethanol. The resultant mixture was then immersed in an iced sonication bath with the addition of ammonia hydroxide NH₄OH (Sigma-aldrich, 28%) as a reaction catalyst to control particle shape and accelerate the reaction. The phosphor particles were washed with ethanol and DI water three times to remove non-reacted residuals and then dried in a 60 °C oven overnight to remove DI water and ethanol. The dried sample was then heated at 500 °C in the air for six hours to remove the volatile and organic residues, and under 1100 °C for three hours with 7% H₂-N₂ gas to reduce the trivalent Eu to the divalent state.

2.2. Sample series

The elemental composition of all samples synthesized in this study was characterized by energy-dispersive X-ray spectroscopy incorporated in an SEM (JSM-IT100, JEOL). They are presented in the form of SiO₂:Al_xEu_y, where *x* and *y* represent the molar percentage (mol%) of Al³⁺ and Eu²⁺, respectively, to all cations (Si + Al + Eu). For instance, sample SiO₂:Al_{0.04}Eu_{0.01} consists of 4 mol% Al³⁺, 1 mol% Eu²⁺, and 95 mol% Si. The synthesized samples are categorized into 3 groups: (I) fixed 4 mol% Al³⁺ concentration (Eu = 0.5, 1, 2, 3 mol%), (II) fixed 1 mol% Eu²⁺ concentration (Al = 1, 2, 3, 4, 10 mol%), and (III) fixed Al/Eu content ratio of 4 (Eu = 1, 3, 5 mol%).

2.3. Luminescent coating production

The coating consists of a dispersing agent, defoamer, acrylic resin, thickeners, and our optimized phosphor. The loading of phosphors was 8 weight% with a wet thickness of 100 μm and applied on a 1 mm sapphire substrate by a bar-coater (TQC film applicator, Industrial Physics). A no-phosphor coating was produced following the same recipe but without phosphor.

2.4. Characterization methods

The crystal structure of samples was checked with X-ray powder diffraction (X'Pert Pro, PANalytical) by using Cu Kα1 radiation. The particle morphology was characterized by a transmission electron microscope (JEM1400, JEOL) and a scanning electron microscope (JSM-IT100, JEOL). The photoluminescence excitation and emission spectra were recorded by a photomultiplier tube (R7600U-20, Hamamatsu) connected to a monochromator (SP2300, Princeton Instruments). A xenon lamp connected to a monochromator (Gemini 180, HORIBA) was used as an excitation light source. All the tested samples were under excitation of 275 nm UV for the measurement of the photoluminescence spectrum (PL), while the photoluminescence excitation spectrum (PLE) was recorded by monitoring emission at 475 nm. The decay spectra were obtained under 275 nm excitation and recorded by a digitizer (DT5730, CAEN) with a pulsed laser (NT230, EKSPLA) as the excitation light source.

The photoluminescence quantum yield (PLQY) of phosphor samples η (%) was determined by integrating over the sample and LED emission wavelength range in an integrating sphere (Labsphere) using a 340 nm LED (M340L4, Thorlabs) excitation light source and a spectrometer (QE65Pro, Ocean Insight) according to the formula:

$$\eta = \frac{\int E_s(\lambda) d\lambda}{\int [R_r(\lambda) - R_s(\lambda)] d\lambda} \quad (1)$$

$R_r(\lambda)$ and $R_s(\lambda)$ are the calibrated reflection spectra of the non-absorbing reference reflector (PTFE, MicroFlon S-203, Shamrock) and the Eu-doped sample respectively under 340 nm excitation while $E_s(\lambda)$ is the calibrated emission spectrum of Eu-doped sample. A commercial phosphor BaMgAl₁₀O₁₇:Eu²⁺ (BAM:Eu, Phosphor Technology) with a reported 90% PLQY was measured in this set-up, and the PLQY of 86.9% was obtained.

2.5. UV to PAR performance indicators

The absorption spectrum $A_s(\lambda)$ (%) and internal UV-to-PAR conversion efficiency η_{coating} (%) of the luminescent coating were characterized by projecting a deuterium light source (AvaLight-DH-S, Avantes) perpendicularly onto the sample. An integrating sphere (Labsphere) was placed behind the sample substrate to collect the transmitted light as shown in Fig. 1. The absorption spectrum $A_s(\lambda)$ and UV-to-PAR conversion efficiency η_{coating} can both be approximated by the formulas:

$$A_s(\lambda) = 1 - \frac{I_{\text{coating}}(\lambda)}{C_{\text{Ref}} * I_{\text{substrate}}(\lambda)} \quad (2)$$

$$\eta_{\text{coating}} = \frac{\int_{400}^{700} [I_{\text{coating}}(\lambda) - C_{\text{Ref}} * I_{\text{substrate}}(\lambda)] d\lambda}{\int_{250}^{400} [C_{\text{Ref}} * I_{\text{substrate}}(\lambda) - I_{\text{coating}}(\lambda)] d\lambda} \quad (3)$$

$I_{\text{substrate}}(\lambda)$ and $I_{\text{coating}}(\lambda)$ are the calibrated intensity spectra of the sapphire substrate and the luminescent coating sample on the sapphire substrate collected by the integrating sphere, respectively. C_{Ref} is a constant that corrects for the difference in reflection with and without coating (caused by surface reflection and diffuse reflection by the particles). The value can be calculated from the transmittance of the coating sample relative to the non-coated sapphire substrate at a wavelength where there is no emission and absorption. A high C_{Ref} value means a

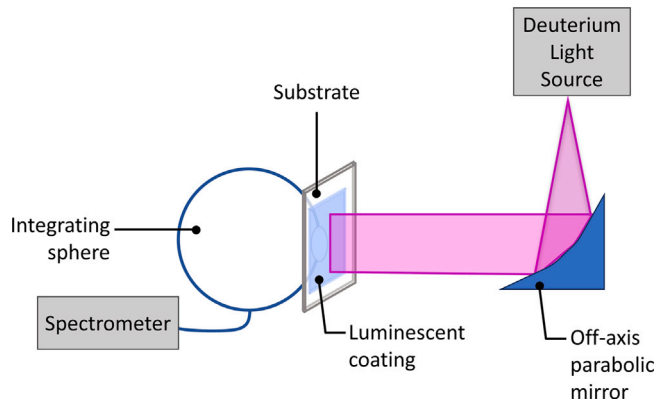


Fig. 1. Illustration of UV to PAR indicators measurement.

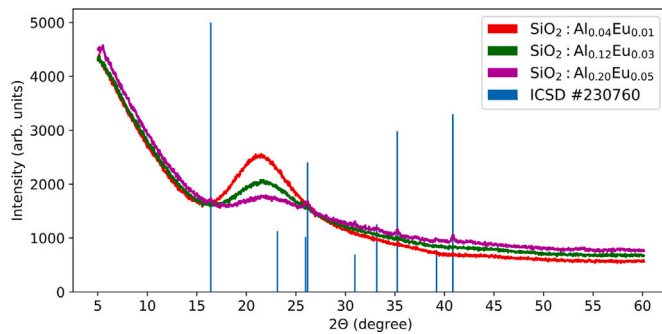


Fig. 2. Recorded XRD pattern of sample $\text{SiO}_2:\text{Al}_{0.04}\text{Eu}_{0.01}$, $\text{SiO}_2:\text{Al}_{0.12}\text{Eu}_{0.03}$, $\text{SiO}_2:\text{Al}_{0.20}\text{Eu}_{0.05}$, and the crystalline silica-alumina oxide reference (ICSD #230760).

small reflection from the coating surface. We make an approximation that C_{Ref} is constant from 250 nm to 800 nm.

To quantify the contribution to extra PAR from the coating sample, we defined the concept of PAR enhancement (%) according to the formula:

$$\text{PAR enhancement} = \frac{\eta_{\text{coating}} * \int_{250}^{400} [A_s(\lambda) * I_{\text{solar}}(\lambda)] d\lambda}{\int_{400}^{700} I_{\text{solar}}(\lambda) d\lambda} \quad (4)$$

The values of $A_s(\lambda)$ and η_{coating} are obtained from Eqs. (2) and (3). $I_{\text{solar}}(\lambda)$ is the AM1.5 solar spectrum in unit of photons derived from ASTM G173-03 Reference Spectra [31]. The calculation of PAR enhancement excludes the influence of the lamp spectrum and utilizes the AM1.5 solar spectrum as a reference, which provides a closer approximation to real-world conditions.

3. Results and discussions

3.1. Crystal structure and morphology

Fig. 2 contains the recorded XRD patterns of $\text{SiO}_2:\text{Al}_{0.04}\text{Eu}_{0.01}$, $\text{SiO}_2:\text{Al}_{0.12}\text{Eu}_{0.03}$, and $\text{SiO}_2:\text{Al}_{0.20}\text{Eu}_{0.05}$. Crystalline features were present only in the highest-doped sample $\text{SiO}_2:\text{Al}_{0.20}\text{Eu}_{0.05}$, matching the crystalline features of a silica-alumina oxide reference (ICSD #230760) indicated by the blue vertical lines, due to high Al^{3+} content in the sample. The rest of the synthesized samples showed only a broad peak at 23 degrees, representing the typical amorphous structure of SiO_2 [32].

The morphology of low-doped and high-doped samples recorded by SEM and TEM are shown in Fig. 3. The size and shape of the low-doped sample were in line with expectations of the base-catalyzed sol-gel approach and confirmed in Fig. 3d [28]. Such morphology disappeared and was replaced by large sharp-edged particles when

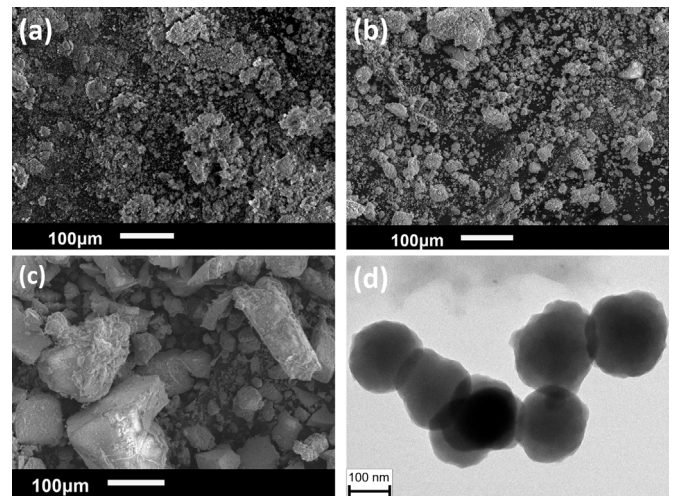


Fig. 3. Morphology of (a) $\text{SiO}_2:\text{Al}_{0.04}\text{Eu}_{0.01}$, (b) $\text{SiO}_2:\text{Al}_{0.12}\text{Eu}_{0.03}$, (c) $\text{SiO}_2:\text{Al}_{0.20}\text{Eu}_{0.05}$. (d) TEM image of the sample $\text{SiO}_2:\text{Al}_{0.04}\text{Eu}_{0.01}$.

dopant/co-dopant content increased (Fig. 3b and c). The particle size increased from a hundred nanometer ($\text{SiO}_2:\text{Al}_{0.04}\text{Eu}_{0.01}$) to 200 nm ($\text{SiO}_2:\text{Al}_{0.20}\text{Eu}_{0.05}$). The SEM images indicate a strong particle agglomeration and irregular shape in the highest-doped sample.

3.2. Luminescence emission, excitation, and absorption spectra

All samples demonstrated a typical photoluminescence excitation spectrum of Eu^{2+} and a broad emission peak, which are attributed to the $4f-5d$ transition of Eu^{2+} [12,13,23]. No characteristic $4f-4f$ line emission of Eu^{3+} was found in any of the emission spectra, indicating that Eu^{3+} was not presented in our samples.

A clear red-shift of the emission peak was observed with increasing Eu^{2+} content in the group I samples (Fig. 4b). This phenomenon is caused by a resonance energy transfer between Eu^{2+} ions [33–35]. The SiO_2 host provides a series of possible sites instead of one specific site for Eu^{2+} due to its amorphous nature and also due to the fact that there is no ion with similar size and charge that Eu^{2+} can replace. The energy released by a donor Eu^{2+} ion with higher energy 5d states, preferably transfers to an acceptor Eu^{2+} ion with lower energy 5d states because of a good spectral overlap between emission of high-energy sites and absorption of low-energy sites. In addition, the energy transfer becomes more efficient when more absorbing centers are presented [36]. As a result, the energy is transferred to Eu^{2+} ions with a lower energy 5d state after multiple transfer steps leading to the observed red-shift of the emission spectra toward higher Eu^{2+} content.

The same type of red-shift was observed in the emission of the fixed-Eu content group (Fig. 4c) following the trend of decreasing Al^{3+} content. The shift is related to the solubility of Eu^{2+} ion in the amorphous SiO_2 host [24–26]. With increasing Al^{3+} content, the distribution of Eu^{2+} ion becomes more homogeneous (clustering is reduced), leading to a longer average distance between Eu^{2+} ions and less energy transfer since the efficiency of energy transfer strongly depends on the atomic distance. Consequently, the resonance energy transfer was suppressed at high-Al content, resulting in a less pronounced red-shift.

In contrast to most of the samples with a similar PLE spectrum as $\text{SiO}_2:\text{Al}_{0.04}\text{Eu}_{0.01}$, the excitation edge of $\text{SiO}_2:\text{Al}_{0.20}\text{Eu}_{0.05}$ showed a more pronounced shift to a longer wavelength (Fig. 4a) due to a high Al^{3+} content and the solvation shell effect [26]. The red-shift of emission peak in the fixed Al/Eu group (Fig. 4d) was a collective result of mechanisms described previously.

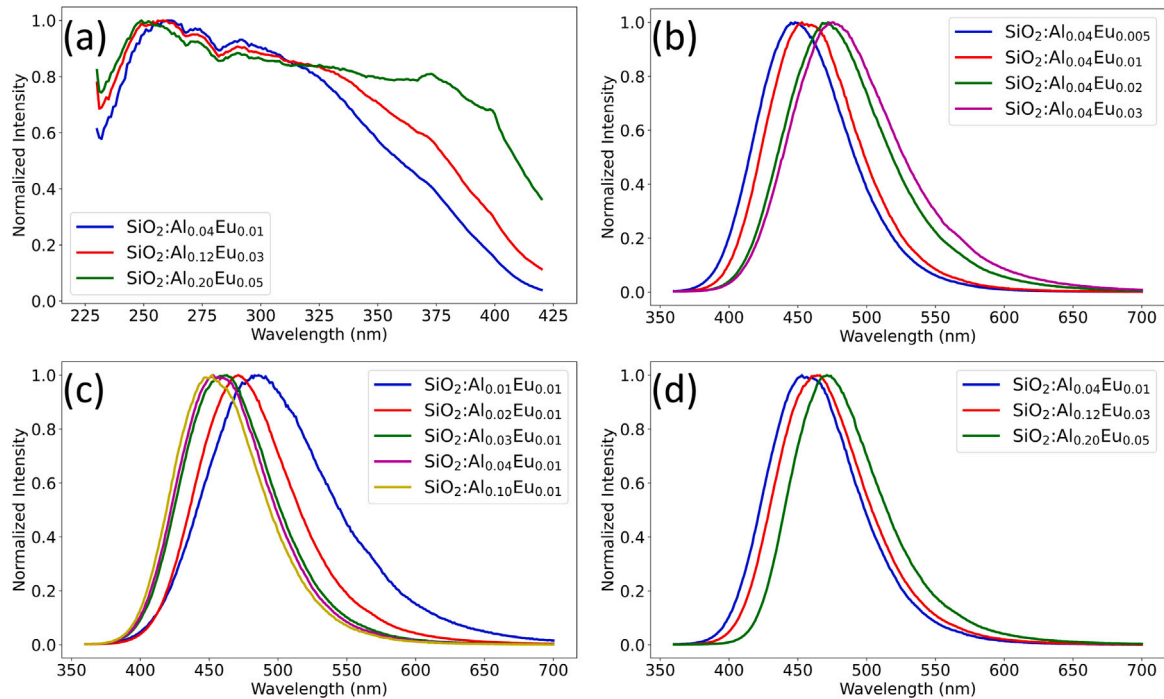


Fig. 4. Photoluminescence excitation (PLE) and photoluminescence (PL) spectra of samples monitored at 475 nm emission and under 275 nm excitation, respectively. (a) PLE spectra of the fixed Al/Eu ratio group. (b) PL spectra of the fixed-Al group. (c) PL spectra of the fixed-Eu group. (d) PL spectra of the fixed Al/Eu ratio group.

3.3. Time-resolved decay characterization

In the fixed-Al group (Fig. 5a), the decay time decreased from 1.72 μ s to 1.29 μ s with increasing Eu²⁺ content due to triggering off concentration quenching effect. The decay spectra of the fixed-Eu group (Fig. 5b) helped find the minimum Al³⁺ content required to avoid shortening luminescent decay time and concentration quenching. Adding more Al³⁺ than 4 mol% had only a slight impact on the decay curve, representing that the solubility of Eu²⁺ ions had been improved to a maximum. These decay curves clearly showed that 4 mol% Al³⁺ is the minimum required amount to dissolve 1 mol% of Eu²⁺ and avoid the Eu²⁺ clustering as well as the unwanted concentration quenching.

Note that when monitoring 475 nm, both the emission of the activator (low-energy Eu²⁺ sites) and the sensitizer (high-energy Eu²⁺ sites) were observed. The relative intensities changed with Eu²⁺ and Al³⁺ content. It is beyond the scope of this work to quantitatively model the complex transfer processes, especially because the nature and number of the Eu²⁺ site distribution is unknown. It is, however, instructive to investigate qualitatively the wavelength dependence of the decay and rise time because it becomes possible to more exclusively

monitor the emission of the activator or the sensitizer. The results of such measurements are shown in Fig. 6.

We expect the high-energy Eu²⁺ ions to act as the sensitizers of the low-energy Eu²⁺ ions, which means that the decay time of the short-wavelength emission (high-energy sites) must be short and a rise time in long-wavelength emissions should be seen. This is indeed observed in Fig. 6a-c. For the low-Al content samples SiO₂:Al_{0.01}Eu_{0.01}, the rise time could not be seen as the decay times were short due to the earlier described efficient energy transfer and concentration quenching in the Eu²⁺ clusters. In high-Al samples, the rapid quenching of short-wavelength emissions diminished due to increased atomic distance between Eu²⁺ ions, resulting in an inefficient energy transfer from the high-energy sites to the low-energy sites and a longer decay time.

The 1/e decay time values of samples in the fixed-Eu group, monitored at wavelengths ranging from 425 nm to 575 nm are summarized in Fig. 6d and compared with BAM:Eu sample. The decay time generally increased with increasing monitored emission wavelength, confirming the earlier explained mechanism of energy transfer among Eu²⁺ ions. The decay time at 425 nm of low-Al samples was one-tenth of that at 575 nm, and one-fourth for the highest-Al sample. The

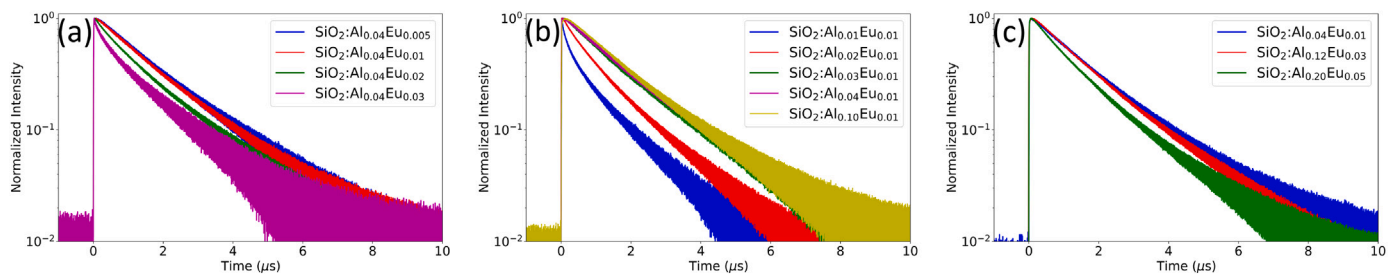


Fig. 5. Decay signal of samples under 275 nm pulse laser excitation and monitored at 475 nm emission. (a) Group I with fixed-Al content. (b) Group II with fixed-Eu content. (c) Group III with fixed Al/Eu ratio.

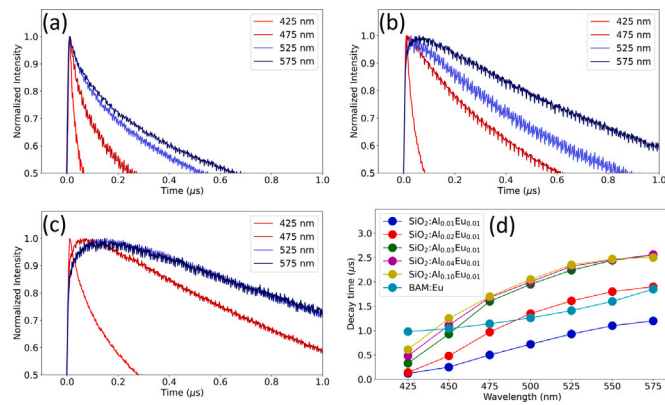


Fig. 6. Wavelength-dependent decay signal under 275 nm pulse laser excitation of (a) $\text{SiO}_2:\text{Al}_{0.01}\text{Eu}_{0.01}$, (b) $\text{SiO}_2:\text{Al}_{0.02}\text{Eu}_{0.01}$, and (c) $\text{SiO}_2:\text{Al}_{0.04}\text{Eu}_{0.01}$. (d) The decay time of fixed-Eu series and reference sample BAM:Eu monitored at various emission wavelengths.

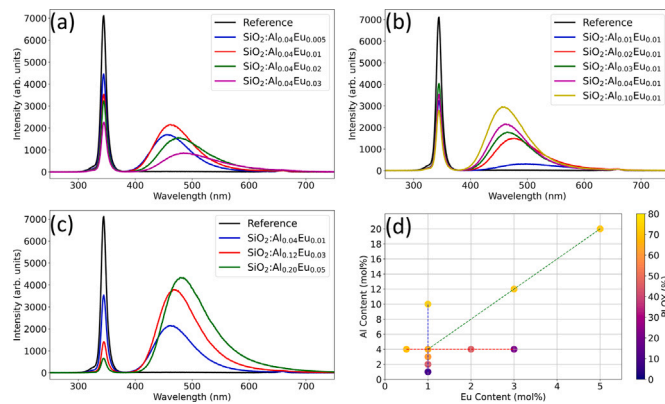


Fig. 7. As-measured UV absorption and emission spectra and photoluminescent quantum yield. (a) Group I with fixed-Al content. (b) Group II with fixed-Eu content. (c) Group III with fixed Al/Eu ratio. (d) Photoluminescent quantum yield of samples grouped by dash lines: red (group I), blue (group II), green (group III).

wavelength-dependent phenomenon was also presented in BAM:Eu, but less pronounced than our samples. The possible reason is that $\text{BaMgAl}_{10}\text{O}_{17}$ provides fewer sites to Eu^{2+} than amorphous SiO_2 [37].

3.4. Photoluminescent quantum yield

Fig. 7 displays the as-measured reflection of 340 nm LED excitation and the respective emission spectra of all samples using an integrating sphere. The absorption of excitation light correlated positively with the Eu^{2+} content in the samples independent from the Al^{3+} content. The shift in emission peaks of each group exhibited the same pattern as Fig. 4. Note that Fig. 7 presents the as-measured spectra instead of calibrated spectra for better visualization. The PLQY calculated based on the calibrated spectra revealed the same trend as observed in the decay spectra. The PLQY value dropped toward a higher Eu^{2+} content from 69% to 21% (group I with fixed-Al content) and dropped toward a lower Al^{3+} content from 74% to 9% (group II with fixed-Eu content). The PLQY of the samples with the fixed Al/Eu ratio (group III) changed marginally from 65% to 72%.

3.5. Luminescent coating performance

Eqs. (2), (3), (4) were developed to quantify the UV to PAR converting efficiency and the PAR enhancement of the luminescent coating and to determine its performance for greenhouse applications. According

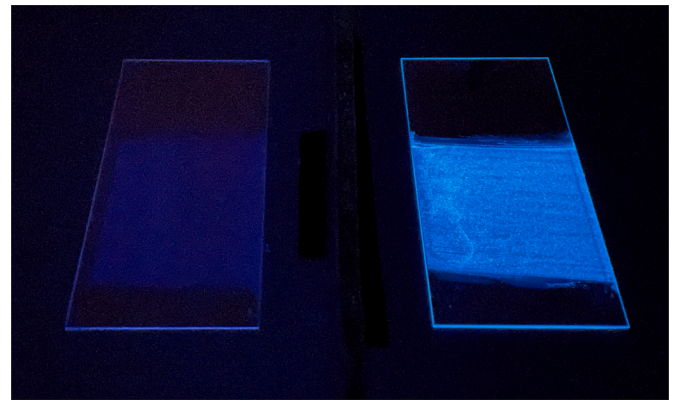


Fig. 8. No-phosphor coating (left) and luminescent coating (right) under 340 nm LED torch.

to Eq. (3), the maximum of η_{coating} is 50% if the selected phosphor has 100% PLQY since only half of the emitted PAR is collected by the integrating sphere located behind the coated samples where the greenhouse would be located. Furthermore, the maximum attainable PAR enhancement is 3.5% if all UV photons below 400 nm in the AM1.5 solar spectrum are converted into PAR and taking into account the 50% η_{coating} .

Based on the PLQY, absorption strength, and emission range, the phosphor $\text{SiO}_2:\text{Al}_{0.12}\text{Eu}_{0.03}$ was selected to produce a luminescent coating that is presented in Fig. 8. The absorption of UV and emission of PAR from the luminescent coating are demonstrated by the transmittance spectra shown in Fig. 9b, which were derived from the calibrated spectra of the sapphire substrate and the coated samples relative to the deuterium light source in Fig. 9a. The luminescent coating absorbed up to 420 nm, matching the excitation spectrum of the selected phosphor $\text{SiO}_2:\text{Al}_{0.12}\text{Eu}_{0.03}$ in Fig. 4d while the absorption below 250 nm was primarily attributed to the polymer matrix. The low transmittance of the luminescent coating outside the emission range (above 650 nm) resulted from the reflection at the coating surface, and hence, the C_{Ref} factor (0.96) was applied in Eqs. (2) and (3). Note that the C_{Ref} is the transmittance of the luminescent coating relative to the non-coated sapphire substrate. The low refractive index of the acrylic-based matrix ($n = 1.49$) led to a higher transmittance of the no-phosphor coating than the non-coated sapphire substrate ($n = 1.76$). The dips at 480, 645, and 655 nm were due to the lamp features.

According to Eq. (3), we obtained a η_{coating} value of 26.2%, whereas a value of 35% was expected since the PLQY of the selected phosphor was 71.5% and only half of the emitted PAR was collected. We assumed the difference lay in the coating layer. First, the polymer matrix absorbed a minor fraction of UV, which was taken into account in the calculation. Second, part of the emitted light was guided to the edges of the coating layer and the substrate, not entering the integrating sphere. In addition, the phosphor absorbing up to 420 nm in the PAR range could also be a potential cause for the underestimated η_{coating} .

Fig. 9a shows a pronounced but unrealistic PAR enhancement from the luminescent coating due to the fact that the deuterium lamp contains a much higher quantity of UV radiation compared to PAR, which is not the case in the AM1.5 spectrum. Therefore, the AM1.5 spectrum was applied in the PAR enhancement calculation, which excluded the influence from the lamp spectrum. Based on Eq. (4), the luminescent coating achieved a 0.34% PAR enhancement, which is low compared to the theoretical maximum of 3.5%. The principal causes for the discrepancy were the less than unity quantum efficiency, UV absorption by the polymer, and the previously described waveguiding effect.

This limited absorption was attributed to the content and excitation properties of Eu^{2+} in the phosphor. The absorption characteristics of

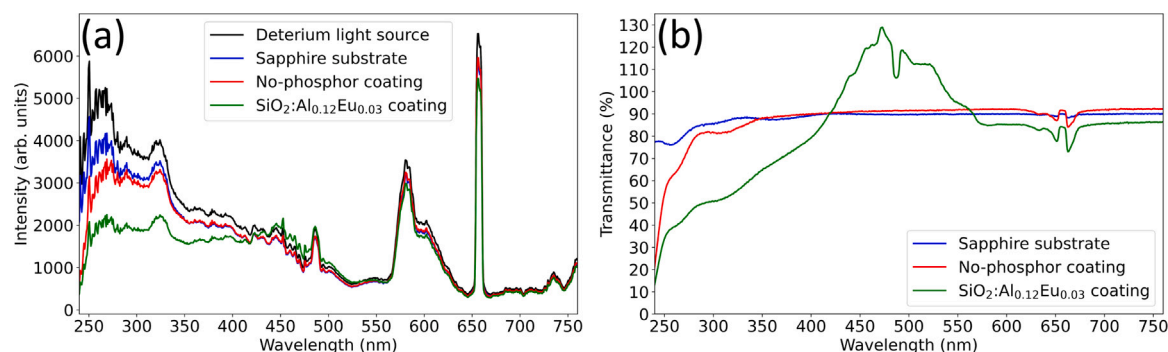


Fig. 9. (a) The calibrated intensity spectra of deuterium light source, non-coated sapphire substrate, no-phosphor coating, and luminescent coating. (b) The transmittance relative to the deuterium light source derived from (a).

the coating depend on intrinsic factors, such as the absorption mechanism of the selected phosphor, and extrinsic factors, such as particle loading and coating thickness. A band gap absorption material generally has a higher absorption strength than the allowed f-d transition which is limited by the content of the activator. Both a higher particle loading and a larger coating thickness can enhance the UV absorption of the coating ($A_s(\lambda)$) and, consequently, the PAR enhancement. However, the surface reflection will increase simultaneously, leading to an undesired low light transmittance in the greenhouse. Future research should focus on optimizing the balance between absorption, PAR emission, and surface reflection to further enhance system efficiency. Overall, our SiO₂:Al_{0.12}Eu_{0.03} luminescent coating obtained one-tenth of the maximum attainable PAR enhancement.

4. Conclusion

SiO₂ phosphors with varying Eu²⁺, varying Al³⁺, and fixed Al/Eu ratio were successfully synthesized to study their potential use as a low-cost UV to PAR spectral conversion coating for greenhouses. A phosphor with a high absorption strength due to a three times higher Eu% and an almost two times higher quantum efficiency compared to the state-of-the-art was achieved by using a base-catalyzed sol-gel method.

Luminescence properties could be explained by assuming energy transfer from high-energy Eu²⁺ sites to low-energy Eu²⁺ sites in the amorphous SiO₂ lattice. For 1 mol% Eu²⁺, a minimum of 4 mol% Al³⁺ is required to avoid Eu²⁺ clustering and minimize energy transfer that causes a red-shift and concentration quenching. The energy transfer phenomena were confirmed by a rise time in the decay curves of the low-energy Eu²⁺ emission and a short decay time of high-energy Eu²⁺ emissions.

A luminescent greenhouse coating based on the phosphor with a high absorption and quantum efficiency (SiO₂:Al_{0.12}Eu_{0.03}) was produced. Despite the optimized absorption and PLQY, the enhanced PAR transmission of the coating was small due to a too low absorption of UV light. We conclude that more efficient spectra conversion coating should, therefore, be based on phosphors that inherently have a much stronger absorption compared to allowed f-d transitions of doping ions such as Eu²⁺. This could be achieved by absorption in the host lattice of materials with band gaps close to 400 nm and strong emission in the PAR range.

CRedit authorship contribution statement

Chun-Ting Cho: Writing – original draft, Methodology, Investigation, Conceptualization. **Giacomo Bosco:** Writing – review & editing. **Erik van der Kolk:** Conceptualization, Methodology, Supervision, Writing – review & editing.

Declaration of competing interest

The authors declare that they have no known competing financial interests or personal relationships that could have appeared to influence the work reported in this paper.

Data availability

No data was used for the research described in the article.

Acknowledgments

This research received funding from the Dutch Research Council (NWO) in the framework of the Science PPP Fund for the top sectors and from the Ministry of Economic Affairs in the framework of the “PPS-Toeslageregeling”.

References

- [1] Food Security Information Network, FSIN and Global Network Against Food Crises. 2023 Mid-Year Update, Tech. Rep., Food Security Information Network, 2023.
- [2] I.J. Mirón, C. Linares, J. Díaz, The influence of climate change on food production and food safety, *Environ. Res.* 216 (2023) 1–6, <http://dx.doi.org/10.1016/j.envres.2022.114674>.
- [3] M.A. Jones, Using light to improve commercial value, *Hortic. Res.* 5 (1) (2018) <http://dx.doi.org/10.1038/s41438-018-0049-7>.
- [4] J.A. Nelson, B. Bugbee, Economic analysis of greenhouse lighting: Light emitting diodes vs. high intensity discharge fixtures, *PLoS One* 9 (6) (2014) <http://dx.doi.org/10.1371/journal.pone.0099010>.
- [5] E. Kaiser, T. Ouzounis, H. Giday, R. Schipper, E. Heuvelink, L.F. Marcelis, Adding blue to red supplemental light increases biomass and yield of greenhouse-grown tomatoes, but only to an optimum, *Front. Plant Sci.* 9 (January) (2019) 1–11, <http://dx.doi.org/10.3389/fpls.2018.02002>.
- [6] C. Gómez, R.C. Morrow, C.M. Bourget, G.D. Massa, C.A. Mitchell, Comparison of intracranial light-emitting diode towers and overhead high-pressure sodium lamps for supplemental lighting of greenhouse-grown tomatoes, *HortTechnology* 23 (1) (2013) 93–98, <http://dx.doi.org/10.21273/horttech.23.1.93>.
- [7] S. Hemming, Use of natural and artificial light in horticulture - interaction of plant and technology, *Acta Hortic.* (907) (2011) 25–35, <http://dx.doi.org/10.17660/ActaHortic.2011.907.1>.
- [8] K.J. McCree, The action spectrum, absorbance and quantum yield of photosynthesis in crop plants, *Agric. Meteorol.* 9 (C) (1971) 191–216, [http://dx.doi.org/10.1016/0002-1571\(71\)90022-7](http://dx.doi.org/10.1016/0002-1571(71)90022-7).
- [9] K. Inada, Action spectra for photosynthesis in higher plants, *Plant Cell Physiol.* 17 (2) (1976) 355–365, <http://dx.doi.org/10.1093/oxfordjournals.pcp.a075288>.
- [10] M. Chen, R.E. Blankenship, Expanding the solar spectrum used by photosynthesis, *Trends Plant Sci.* 16 (8) (2011) 427–431, <http://dx.doi.org/10.1016/j.tplants.2011.03.011>.
- [11] D. Kim, Y.-H. Jin, K.-W. Jeon, S. Kim, S.-J. Kim, O.H. Han, D.-K. Seo, J.-C. Park, Blue-silica by Eu²⁺-activator occupied in interstitial sites, *RSC Adv.* 5 (91) (2015) 74790–74801, <http://dx.doi.org/10.1039/C5RA15641F>.
- [12] P. Dorenbos, Energy of the first 4f⁷ → 4f⁶5d transition of Eu²⁺ in inorganic compounds, *J. Lumin.* 104 (4) (2003) 239–260, [http://dx.doi.org/10.1016/S0022-2313\(03\)00078-4](http://dx.doi.org/10.1016/S0022-2313(03)00078-4).

- [13] M. Nogami, T. Yamazaki, Y. Abe, Fluorescence properties of Eu^{3+} and Eu^{2+} in Al_2O_3 - SiO_2 glass, *J. Lumin.* 78 (1) (1998) 63–68, [http://dx.doi.org/10.1016/S0022-2313\(97\)98281-8](http://dx.doi.org/10.1016/S0022-2313(97)98281-8).
- [14] M. Nogami, Y. Abe, Properties of sol–gel-derived Al_2O_3 - SiO_2 glasses using Eu^{3+} ion fluorescence spectra, *J. Non-Cryst. Solids* 197 (1) (1996) 73–78, [http://dx.doi.org/10.1016/0022-3093\(95\)00621-4](http://dx.doi.org/10.1016/0022-3093(95)00621-4).
- [15] N.J.J. Johnson, S. He, S. Diao, E.M. Chan, H. Dai, A. Almutairi, Direct evidence for coupled surface and concentration quenching dynamics in lanthanide-doped nanocrystals, *J. Am. Chem. Soc.* 139 (8) (2017) 3275–3282, <http://dx.doi.org/10.1021/jacs.7b00223>.
- [16] S. Sen, J. Stebbins, Structural role of Nd^{3+} and Al^{3+} cations in SiO_2 glass: a ^{29}Si MAS-NMR spin-lattice relaxation, ^{27}Al NMR and EPR study, *J. Non-Cryst. Solids* 188 (1–2) (1995) 54–62, [http://dx.doi.org/10.1016/0022-3093\(95\)00099-2](http://dx.doi.org/10.1016/0022-3093(95)00099-2).
- [17] M.J. Lochhead, K.L. Bray, Rare-earth clustering and aluminum codoping in Sol-Gel silica: investigation using europium(III) fluorescence spectroscopy, *Chem. Mater.* 7 (3) (1995) 572–577, <http://dx.doi.org/10.1021/cm00051a019>.
- [18] K. Arai, H. Namikawa, K. Kumata, T. Honda, Y. Ishii, T. Handa, Aluminum or phosphorus co-doping effects on the fluorescence and structural properties of neodymium-doped silica glass, *J. Appl. Phys.* 59 (10) (1986) 3430–3436, <http://dx.doi.org/10.1063/1.336810>.
- [19] Z. Pan, H. He, R. Fu, S. Agathopoulos, X. Song, Influence of Ba^{2+} -doping on structural and luminescence properties of $\text{Sr}_2\text{SiO}_4:\text{Eu}^{2+}$ phosphors, *J. Lumin.* 129 (9) (2009) 1105–1108, <http://dx.doi.org/10.1016/j.jlumin.2009.05.011>.
- [20] M.O. Onani, P. Mushonga, L.F. Koao, F.B. Dejene, Luminescence properties of Eu- and Mg-codoped Sol-Gel glasses, *ISRN Nanotechnol.* 2012 (2012) 1–5, <http://dx.doi.org/10.5402/2012/298694>.
- [21] H. Fneich, N. Gaumer, S. Chausseidant, W. Blanc, A. Mehdi, Europium-doped sol-gel SiO_2 -based glasses: effect of the europium source and content, magnesium addition and thermal treatment on their photoluminescence properties, *Molecules* 23 (7) (2018) 1768, <http://dx.doi.org/10.3390/molecules23071768>.
- [22] P. Jaffe, Eu^{2+} luminescence in the ternary $\text{EuO-Al}_2\text{O}_3\text{-SiO}_2$ system, *J. Electrochem. Soc.* 16 (155) (1969) <http://dx.doi.org/10.1149/1.2411991>.
- [23] M. Nogami, Y. Abe, Enhanced emission from Eu^{2+} ions in sol-gel derived Al_2O_3 - SiO_2 glasses, *Appl. Phys. Lett.* 69 (25) (1996) 3776–3778, <http://dx.doi.org/10.1063/1.116995>.
- [24] Y. Kishimoto, X. Zhang, T. Hayakawa, M. Nogami, Blue light emission from Eu^{2+} ions in sol-gel-derived Al_2O_3 - SiO_2 glasses, *J. Lumin.* 129 (9) (2009) 1055–1059, <http://dx.doi.org/10.1016/j.jlumin.2009.04.031>.
- [25] J. Lægsgaard, Dissolution of rare-earth clusters in SiO_2 by al codoping: A microscopic model, *Phys. Rev. B* 65 (17) (2002) 174114, <http://dx.doi.org/10.1103/PhysRevB.65.174114>.
- [26] F. Funabiki, T. Kamiya, H. Hosono, Doping effects in amorphous oxides, *J. Ceram. Soc. Japan* 120 (1407) (2012) 447–457, <http://dx.doi.org/10.2109/jcersj2.120.447>.
- [27] A. Patra, E. Sominska, S. Ramesh, Y. Kolytyn, Z. Zhong, H. Minti, R. Reinfeld, A. Gedanken, Sonochemical preparation and characterization of Eu_2O_3 and Tb_2O_3 doped in and coated on silica and alumina nanoparticles, *J. Phys. Chem. B* 103 (17) (1999) 3361–3365, <http://dx.doi.org/10.1021/jp9847661>.
- [28] I. Rahman, P. Vejayakumaran, C. Sipaut, J. Ismail, C. Chee, Size-dependent physicochemical and optical properties of silica nanoparticles, *Mater. Chem. Phys.* 114 (1) (2009) 328–332, <http://dx.doi.org/10.1016/j.matchemphys.2008.09.068>.
- [29] S.K. Jakka, M.M. Silva, M.J. Soares, K. Pavani, Exploring the potential of Eu^{3+} and Mn^{4+} activated LaAlO_3 phosphors as red and far-red emitters for horticulture lighting, *RSC Adv.* 13 (45) (2023) 31314–31320, <http://dx.doi.org/10.1039/d3ra03241h>.
- [30] K. Mishra, C. Stanghellini, S. Hemming, Technology and materials for passive manipulation of the solar spectrum in greenhouses, *Adv. Sustain. Syst.* 7 (5) (2023) <http://dx.doi.org/10.1002/advs.202200503>.
- [31] C.A. Gueymard, D. Myers, K. Emery, Proposed reference irradiance spectra for solar energy systems testing, *Sol. Energy* 73 (6) (2002) 443–467, [http://dx.doi.org/10.1016/S0038-092X\(03\)00005-7](http://dx.doi.org/10.1016/S0038-092X(03)00005-7).
- [32] X. Chen, J. Jiang, F. Yan, S. Tian, K. Li, A novel low temperature vapor phase hydrolysis method for the production of nano-structured silica materials using silicon tetrachloride, *RSC Adv.* 4 (17) (2014) 8703–8710, <http://dx.doi.org/10.1039/c3ra47018k>.
- [33] D. de Graaf, H.T. Hintzen, S. Hampshire, G. de With, Long wavelength Eu^{2+} emission in Eu-doped Y-Si-Al-O-N glasses, *J. Eur. Ceram. Soc.* 23 (7) (2003) 1093–1097, [http://dx.doi.org/10.1016/S0955-2219\(02\)00236-4](http://dx.doi.org/10.1016/S0955-2219(02)00236-4).
- [34] P.R. Selvin, T.M. Rana, J.E. Hearst, Luminescence resonance energy transfer, *J. Am. Chem. Soc.* 116 (1994) 6029–6030, <http://dx.doi.org/10.1021/ja00092a088>.
- [35] C.Y. Wang, T. Takeda, O.M. Ten Kate, R.J. Xie, K. Takahashi, N. Hirosaki, Synthesis and photoluminescence properties of a phase pure green-emitting Eu doped JEM sialon ($\text{LaSi}_{6-z}\text{Al}_{1+z}\text{N}_{10-z}\text{O}_z$, $z \leq 1$) phosphor with a large red-shift of emission and unusual thermal quenching behavior, *J. Mater. Chem. C* 4 (43) (2016) 10358–10366, <http://dx.doi.org/10.1039/c6tc02229d>.
- [36] E.P. Merckx, S. van Overbeek, E. van der Kolk, Functionalizing window coatings with luminescence centers by combinatorial sputtering of scatter-free amorphous SiAlON:Eu²⁺ thin film composition libraries, *J. Lumin.* 208 (2019) 51–56, <http://dx.doi.org/10.1016/j.jlumin.2018.12.011>.
- [37] K.-B. Kim, Y.-I. Kim, H.-G. Chun, T.-Y. Cho, J.-S. Jung, J.-G. Kang, Structural and optical properties of $\text{BaMgAl}_{10}\text{O}_{17}:\text{Eu}^{2+}$ phosphor, *Chem. Mater.* 14 (12) (2002) 5045–5052, <http://dx.doi.org/10.1021/cm020592f>.